ACI STRUCTURAL JOURNAL TECHNICAL PAPER

Title No. 121-S72

Prestressing Analysis of Large Three-Dimensional Systems and Prestress Management

by Hiroshi Nishio, Yosuke Yagi, and Yasuaki Ishikawa

A three-dimensional (3-D) finite element method for prestressing and seating analysis has been developed. This method improves the accuracy of the results obtained using the widely adopted initial stress method and enables calculation of the seating loss effect, which is the final stress prediction of prestressing. Its application for large numbers of indeterminate-order structures is shown by comparing its calculation results with two-dimensional (2-D) conventional analysis, as well as with observed strain results for cables of an existing 462 m, six-span continuous bridge. With these considerations, a new management method of prestressing for jack force-diverting systems where the prestressing force does not focus uniquely on a design section was developed so that constructed prestressed concrete structures can be well-secured to comply with design objectives.

Keywords: friction loss; large-scale prestressed concrete (PC) structure; prestressing analysis; prestressing management; set loss; three-dimensional (3-D) finite element method (FEM) analysis.

INTRODUCTION

The three-dimensional (3-D) finite element method (FEM) analysis of prestressing is usually performed with the initial stress method, as found in software programs such as Abaqus and DIANA. However, this method has fundamental shortcomings, such as cable rigidity affecting the accuracy of calculations and setting common joints between cables, and concrete does not allow relative slip between the two, although slip is a known phenomenon. DIANA has provided a remedy in which the rigidity of cables is made ineffective during prestressing and retrieved after grouting. In contrast, Abaqus ignores these deficiencies by assuming that their effects are negligibly small.

These findings were reviewed in a previous paper[1] that pointed out that the stress error amounts to several tens of percent of the actual values when the relative rigidity ratio between concrete and cables becomes large.

This study developed a more direct method to obtain the prestressing load for concrete that can overcome the aforementioned deficiencies of the initial stress method and also developed an improved analysis method for seating loss that gives more accurate results than the initial stress method adopted in software such as DIANA.[2]

The developed method also makes possible the calculation of pulled-out cable lengths from anchorage plates at prestressing, the value of which is used for prestressing management in a more advanced manner. Then, the applicability of the developed prestress calculation method for a large degree-of-freedom system, including the calculation of stress variation at the seating stage of prestressing, is shown with observed stresses for an actual elevated s-curved bridge having a length of 462 m. The results obtained for 3-D reaction forces and moments for piers and box girders are considered to be important design variables for this type of bridge but cannot be determined using a two-dimensional (2-D) frame analysis, although the use of 2-D frame analysis is currently specified in the standards for bridge construction in Japan[3] for a treated s-curved multi-span bridge.

Basing on the results obtained in this study, an advanced management method for prestressing is proposed.

RESEARCH SIGNIFICANCE

The developed 3-D FEM was applied to prestressing analysis of an existing six-span curved prestressed concrete (PC) bridge 462 m long, and the results of the examination assured its applicability to general cases of prestressing analysis of any 3-D structures with an arbitrary cable layout. Based on these results, this paper proposes a more accurate prestressing management method, which is expected to contribute to improved PC construction quality.

THEORETICAL CONSIDERATION OF PRESTRESSING AND SEATING ANALYSIS

The prestressing cable force exerted on concrete is given directly by the differential of the cable force along its length, which improves the accuracy of the initial stress method for prestressing analysis and seating loss analysis for final prestress prediction.

Prestressing analysis

The cable force vector $\boldsymbol{T}$ that acts on concrete depends on the cable configuration and is expressed generally as

$$\boldsymbol{T}(\theta,s) = T(\theta,s) \cdot \boldsymbol{n} \tag{1}$$

The force vector $\boldsymbol{f}$ acting on concrete is the variation of the cable force and given in differential form as

$$\boldsymbol{f} = \frac{\partial \boldsymbol{T}(\theta,s)}{\partial s} = \frac{\partial T(\theta,s) \cdot \boldsymbol{n}}{\partial s} = \frac{\partial T(\theta,s)}{\partial s} \cdot \boldsymbol{n} + T(\theta,s)\frac{\partial \boldsymbol{n}}{\partial s} = \boldsymbol{S} + \boldsymbol{Z} \tag{2}$$

ACI Structural Journal, V. 121, No. 5, September 2024.
MS No. S-2023-170.R2, doi: 10.14359/51740857, received February 29, 2024, and reviewed under Institute publication policies.

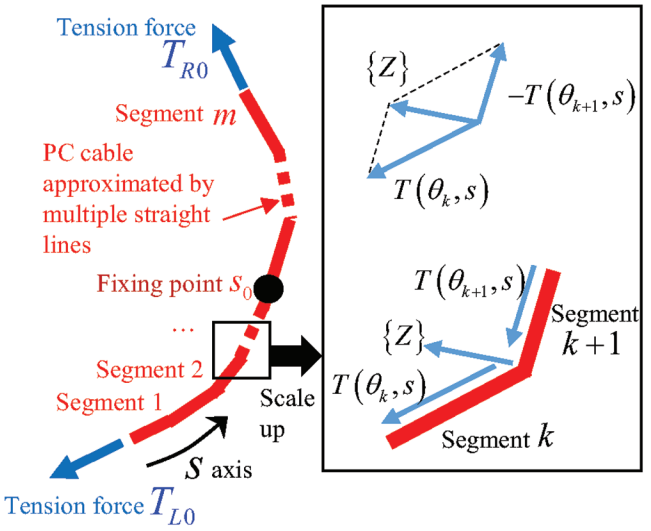

Fig. 1—Approximation of curved PC cable by multiple straight lines.

where

$$\boldsymbol{S} = \frac{\partial T(\theta,s)}{\partial s} \cdot \boldsymbol{n} \tag{3}$$

and

$$\boldsymbol{Z} = T(\theta,s)\frac{\partial \boldsymbol{n}}{\partial s} \tag{4}$$

where $\boldsymbol{n}$ is the directional normal along the coordinate s of the cable configuration. The first term on the right-hand side of Eq. (2) is the frictional force, and the second term is the pseudo-centripetal force.

To treat these forces numerically, a PC cable with a curved configuration in 3-D space is approximated by multiple straight lines and modeled as a series of line groups composed of m line segments, as shown in Fig. 1, the length of which depends on the required solution accuracy. The length of m line segments is generally not equally divided, and it is necessary to divide it depending on the PC cable curvature radius. In a domain where the curvature radius is small, it is necessary to increase the number of divisions and use a small line segment length. Note that both ends of each line segment need not be on the surface of solid elements of concrete. Let coordinate s along the line segment be taken from the left end of the PC steel, and let θ_k be the sum of the angles formed by line segments $k+1$ from the left contacting end, where the angle is measured clockwise. Then, Eq. (3) is reduced to

$$\{S\} = \frac{\partial T(\theta_k,s)}{\partial s}\{n_k\} \tag{5}$$

where $\{n_k\}$ denotes the unit vector for the direction of the line segment k. When an angle change occurs between line segment k and line segment $k+1$, as shown in Fig. 2, the pseudo-centripetal force $\{Z\}$ in Eq. (4) is reduced to

$$\{Z\} = T(\theta_k,s)\{n_k\} - T(\theta_{k+1},s)\{n_{k+1}\} \tag{6}$$

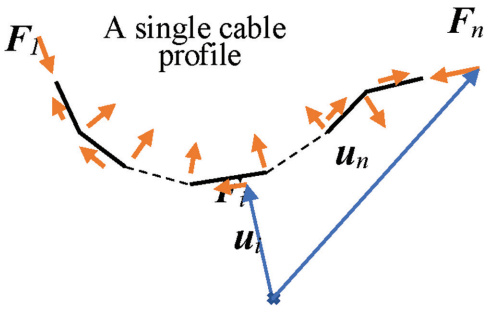

Fig. 2—Forces equivalent to prestressing effect.

This force is converted to the nodal force for 3-D elements by applying the virtual work principle.

Error norm of discretized joint forces

Forces working on concrete with cable prestressing are reactions in concrete that occur against the jack pulling, frictional, and pseudo-centripetal forces, as shown in Fig. 2. These forces are always self-balancing for every cable; therefore, the forces and the moments satisfy the following equations in each cable

$$\sum \boldsymbol{F}_i = 0, \sum \boldsymbol{F}_i \times u_i = 0 \tag{7}$$

where $\boldsymbol{F}_i$ is the combined jack, frictional, and other forces; and $\boldsymbol{u}_i$ may be measured from any point in space.

Now, in the construction of an actual bridge, several hundred cables would be used with prestressing forces of 1000 to 3000 kN for each cable. When the FEM calculation is applied, these forces, which are reacting to the cable forces, are converted to nodal forces of elements and denoted as

$$N_x, N_y, N_z \tag{8}$$

for each joint of the elements through which cables pass. Though the equation should satisfy

$$\sum N_{x,i} = 0, \sum N_{y,i} = 0, \sum N_{z,i} = 0$$

and

$$\sum(yN_z - zN_y) = 0, \sum(zN_x - xN_z) = 0, \sum(xN_y - yN_x) = 0 \tag{9}$$

this is not the case, and errors always exist

$$\sum N_x = \Delta_x, \sum N_y = \Delta_y, \sum N_z = \Delta_z$$
$$\sum(yN_z - zN_y) = \Delta_{mx}, \sum(zN_x - xN_z) = \Delta_{my}, \sum(xN_y - yN_x) = \Delta_{mz} \tag{10}$$

Therefore, the error norms are defined as

$$N_{rm}N_x = \frac{\Delta_x}{\sum|N_x|}, \quad N_{rm}N_y = \frac{\Delta_y}{\sum|N_y|}, \quad N_{rm}N_z = \frac{\Delta_z}{\sum|N_z|}$$

$$N_{rm}M_x = \frac{\Delta_{mx}}{\sum|(yN_z - zN_y)|}$$

$$N_{rm}M_y = \frac{\Delta_{my}}{\sum|(zN_x - xN_z)|}$$

$$N_{rm}M_z = \frac{\Delta_{mz}}{\sum|(xN_y - yN_z)|} \quad (11)$$

Depending on the magnitude of the error norm, redistribution of the nodal force should be considered, and its limit may be given by the required calculation accuracy. However, the limits of error norm may be set at approximately 10^{-3} to 10^{-5} in general cases. In the following discussion, the error norm is found to be below 10^{-3} in all cases, and no redistribution of the nodal forces is performed.

Seating loss analysis

Seating loss analysis requires calculating pulled-out cable lengths at the ends, where cable extension and concrete deformation calculations are necessary.

To obtain the pulled-out cable lengths from anchor plates at the left and right ends, it is necessary to consider deformation of concrete along the cable profile as well as the amount of PC steel extension, as shown in Fig. 3. Pulled-out cable lengths at both ends are expressed by the following equations, where the lengths at the left and right ends are denoted as Δl_L and Δl_R, respectively

$$\Delta l_L = \Delta l_{L,cab} - \Delta l_{L,con} \quad (12a)$$

$$\Delta l_R = \Delta l_{R,cab} - \Delta l_{R,con} \quad (12b)$$

where the subscripts *cab* and *con* denote components of the pulled-out length attributed to PC cable extension and concrete deformation, respectively.

The left and right pulled-out lengths for a PC cable can be expressed by the following equations, respectively, by the path integral of the strain generated in the PC cable along the cable length starting from the unmovable fixing point to the left or right end

$$\Delta l_{L,cab} = \int_0^{s_0} \frac{T(\theta_k, s)}{EA} ds \quad (13a)$$

$$\Delta l_{R,cab} = \int_{s_0}^{l_{end}} \frac{T(\theta_k, s)}{EA} ds \quad (13b)$$

where EA is the axial stiffness of the PC cable; s_0 is the unmovable fixing point of a cable; and l_{end} is the total cable length.

In addition, the left and right pulled-out cable length components due to concrete contraction are expressed by Eq. (14a) and (14b), respectively, by the path integral of concrete strain components along the PC cable from the unmovable fixing point s_0 to the left or right end

$$\Delta l_{L,con} = \int_0^{s_0} \varepsilon_c ds \quad (14a)$$

$$\Delta l_{R,con} = \int_{s_0}^{l_{end}} \varepsilon_c ds \quad (14b)$$

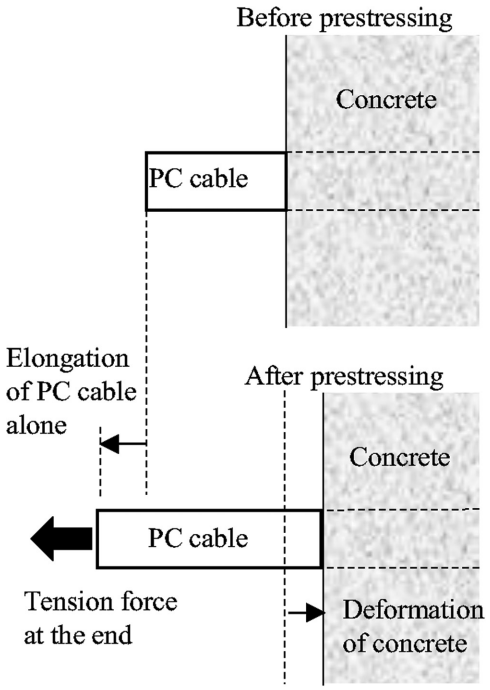

Fig. 3—Pulled-out PC cable length including concrete.

where ε_c is a normal strain component for concrete in the direction along the PC cable and is expressed by Eq. (15) using the concrete strain tensor ε_{ij} and the component n_i of the unit vector $\{n_k\}$.

$$\varepsilon_c = \varepsilon_{ij} n_i n_j \quad (15)$$

Let q_L and q_R be the seating length values for the left and right ends, respectively, for a PC cable due to anchor seating. The solution for the problem requires the iterations given as follows.

In the first step, these deformations are assumed to be composed of components of the PC cable extension alone. From Eq. (13), q_L and q_R can be expressed as

$$q_L = \int_0^{s_0} \frac{T(\theta_k, s)}{EA} ds \quad (16a)$$

$$q_R = \int_{s_0}^{s_{max}} \frac{T(\theta_k, s)}{EA} ds \quad (16b)$$

In writing Eq. (16a) and (16b), the tension force relief at both ends may be different and accompanied by arbitrary anchor-seating magnitudes. If the tension force at the fixing point is given as T_{s0}, the tension force distribution due to the anchor-seating reliefs can be expressed by the following expressions from Eq (1)

$$T(\theta_k, s) = \begin{cases} T_{s_0} \cdot e^{\mu\theta_k + \lambda s} & s \le s_0 \\ T_{s_0} \cdot e^{\mu\theta_{m-k} + \lambda(s_{max} - s)} & s > s_0 \end{cases} \quad (17)$$

It should be noted that the fixing point position for Eq. (17) will be generally different from that for the tensioning process. Substitution of Eq. (17) into Eq. (16) yields two unknown variables, T_{s_0} and s_0, for the given values of

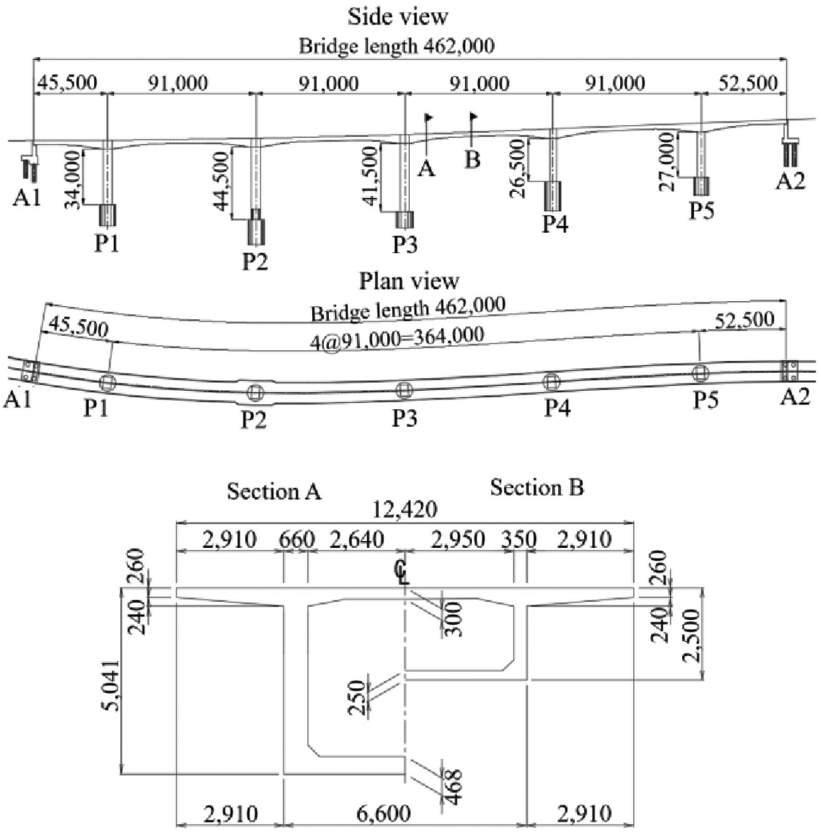

Fig. 4—General view of target existing continuous viaduct. (Note: Units are in mm.)[4]

Eq. (16). The obtained T_{s_0} and s_0 are used to find the equivalent nodal force due to the anchor-seating loss in the same way as described in the previous section. After solving the global stiffness equation, the new concrete contraction deformation is recalculated in the same way as described in the previous section, and then the pulled-out lengths for the PC cable are updated using the following equations

$$\Delta l_{L,con} = q_L + \Delta l_{L,con} \tag{18a}$$

$$\Delta l_{R,con} = q_R + \Delta l_{R,con} \tag{18b}$$

This process is repeated until the deformation converges.

It should be noted that a new friction coefficient at the seating stage should be identified, even when holding the superposition assumption of cable force derivation at this stage.

So far, the cable forces are considered to correspond to those on the concrete. Therefore, the rigidity of the cables is not considered in the FEM stiffness calculation. However, to calculate the stress after seating, it is necessary to consider the cable stiffness in the cases of full or partial bonding to concrete. Such an unbonded prestressing analysis is another theoretical problem and is under study by the authors.

SIMULATION BY PROPOSED 3-D FEM OF EXISTING CONTINUOUS VIADUCT AT PRESTRESSING AND COMPARISON WITH CONVENTIONAL CALCULATION RESULTS

Overview of existing viaduct and outline of study

Figure 4 shows the shape, longitudinal view, and plan view of the existing bridge. The total length is 462 m, and the curved section is approximately 12 m away from the straight line connecting A1 and A2 at the point of greatest curvature. An elevation difference of approximately 5 m exists between A1 and A2 due to a longitudinal gradient. Table 1 shows the dimensions of the bridge.

The specific response for this bridge was studied assuming simultaneous prestressing of all the external cables placed between A1 and A2 to compare the results of the proposed method, conventional analysis, and actual measurements. Prestressing cables with built-in optical fibers in the external cables[4,5] were specially arranged between P2 and P4 and between P1 and P2, and the tension force of the cables was measured. These cable forces observed at prestressing and after seating were compared with the calculated results.

Figure 5 shows a diagram of the analysis model for the proposed method and a part of the discretization. Table 2 shows the parameters used for the analysis. Because the bridge draws a gentle s-curve on the plane and has a gentle upward slope from A1 to A2, the arrangement of the prestressing cables is not symmetric. In the analysis by the proposed method, the whole bridge (462 m long, six spans) was faithfully discretized, as shown in Fig. 5. Therefore, it was a large degree-of-freedom analysis with 257,566 elements, 367,271 nodes, and 1,101,813 degrees of

Table 1—Overview of target existing continuous viaduct

Bridge type	PC box-girder bridge
Structural form	Six-span continuous rigid-frame viaduct
Bridge length	462.000 m (road center)
Span length	44.500 + 4 @ 91.000 + 51.500 m (structural center)
Width	12.800 to 15.300 m
Effective width	5.565 + 5.565 to 6.815 + 6.815
Bridge alignment	Longitudinal gradient: +3.007% (L = 470.000 m)
	Cross slope: 1.886 to 6.000%
	Plane figure: A = 400 to 450 m (clothoid) to R = 900 m (arc)

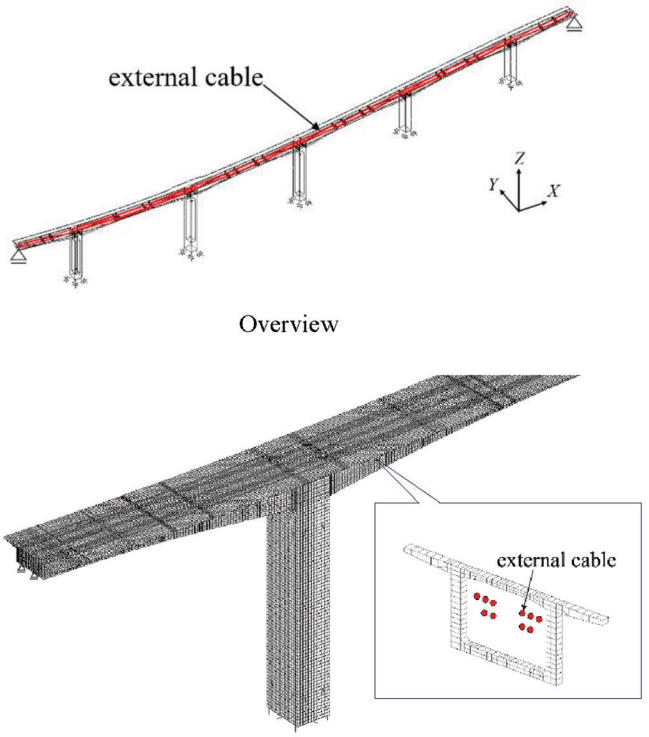

Fig. 5—Analysis model for proposed method.

freedom. The calculation time was approximately 2 hours with a processor at 3.70 GHz, with 128 GB of installed random-access memory (RAM). It is noted that the calculation time was relatively short because the prestressing analysis was linear.

Bridge deformation and stress distribution due to simultaneous prestressing of all external cables

Prestressing load on concrete—As shown in Fig. 6 and Table 3, the five sets of external cables are arranged to extend over two span lengths in each set and overlap at every span. The number of cables in each set and the prestressing forces are shown in Table 3; the total tension force was approximately 96,000 kN.

Table 2—Parameters used for analysis

Young's modulus	Concrete (superstructure)	31,000 N/mm^2
	Concrete (substructure)	28,000 N/mm^2
	Prestressing cable (from mill sheet)	194,150 N/mm^2
Coefficient of friction	Per length	0/m
	Per angle	0.3/rad
Analysis model	Number of nodes	367,271
	Number of elements	257,566

Table 3—Overview of external cable arrangement

Cable position		A1 to P2	P1 to P3	P2 to P4	P3 to P5	P4 to A2
Cable piece		6	6	4	6	6
Final prestressing, kN/piece	A1 side	3254.6				
	A2 side	3254.6				
Coefficient of friction	μ	0.3				
	λ	0				
Pulled-out length at anchorage, mm	A1 side	5.0				
	A2 side	5.0				

As an example of discrete prestressing load derivation, one cable out of four at the span P2 to P4, the profile of which is shown in Fig. 7, was selected, and the frictional load in the x-direction and centripetal load in the y- and z-directions were calculated when prestressing with a jack force of 3254.6 kN was applied at both ends, as shown in Fig. 8, to demonstrate the characteristics of this method. It should be noted that it is difficult to determine these values using the initial stress method. These prestressing loads are shown along the cable profile in such a manner that slack is removed from the curved profile length to form a straight line. The load peaks are at diaphragm wall locations inside the box-section girder because the cable is an external cable. This figure shows that the prestressing force applies a rather peculiar load that acts on the bridge horizontally in both the x- and y-directions, as well as vertically. Therefore, the bridge response depends on these forces and deforms accordingly. In addition, the loads shown in Fig. 8 and the jack force of 3254.6 kN at both ends make up the total prestressing load, and their summed values are equal to the summed reaction forces at the pier bases.

Deformation and sectional stress—The actual prestressing timing differs for each cable, but the analysis by the conventional calculation of prestressing was performed assuming simultaneous prestressing of all sets of cables. Here, it is noted that the conventional method, as described in the present paper, denotes the method actually used in the design and documented in the design of the bridge analyzed herein, the model of which is a 2-D frame analysis with the initial strain method. The theoretical manual for the software used is referred to as UC-BRIDGE[6] or PCBOX-II.[7]

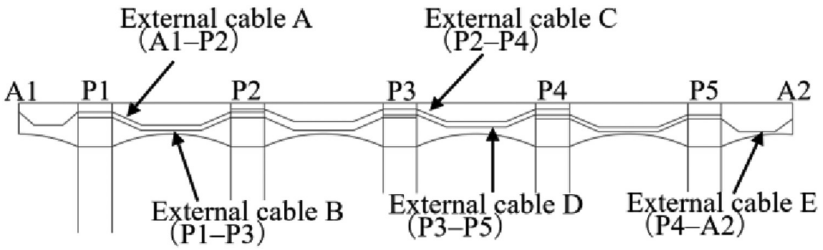

Fig. 6—Schematic diagram of external cable layout.

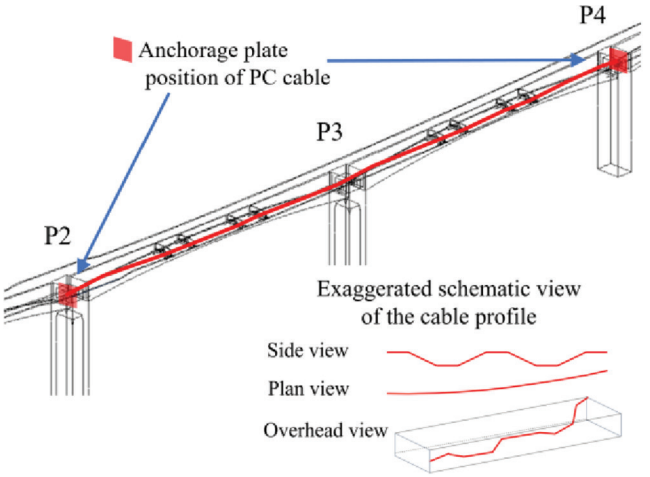

Fig. 7—Analysis model of P2 to P4 external cable prestressing.

Therefore, the calculated results are first compared with the 2-D frame analysis results, using the same parameters in both cases, such as the friction coefficient and Young's modulus of the materials.

Table 4 compares the calculated sectional forces, and Table 5 compares the displacement results. Though a difference exists in the displacements in the x- and z-directions, the most striking difference between the two methods is the displacement in the y-direction, which is normal to the bridge axis. The conventional calculation does not provide this information because it is a 2-D calculation. It is interesting that the deformation makes an inverted s-curve in the horizontal plane, which is reasonable.

Similarly, Fig. 9(b), (d), and (e) provide information that is not obtained in a conventional 2-D calculation. Because the prestressing cable profile has a nearly s-shaped curve in the direction of the bridge axis, a pseudo-centripetal positive horizontal force is acting on it, which is followed by the negative horizontal pseudo-centripetal force. Therefore, Fig. 9(b) shows that the piers are deflecting in the reverse s-curve direction; the reaction force directions in Fig. 9(b) show them at the base of each pier. Figure 9(d) also shows the 3-D effect of the prestressing—that is, the moment around the x-axis—which does not appear in the 2-D conventional calculation.

Figure 9(c) shows the uplifting force acting on the piers due to prestressing, which can be calculated by both the conventional and proposed methods. However, the prestressing induction that uplifts the structures is a rather peculiar external force. These indications show that, in general, 3-D effects can never be neglected for curvilinear bridge shapes.

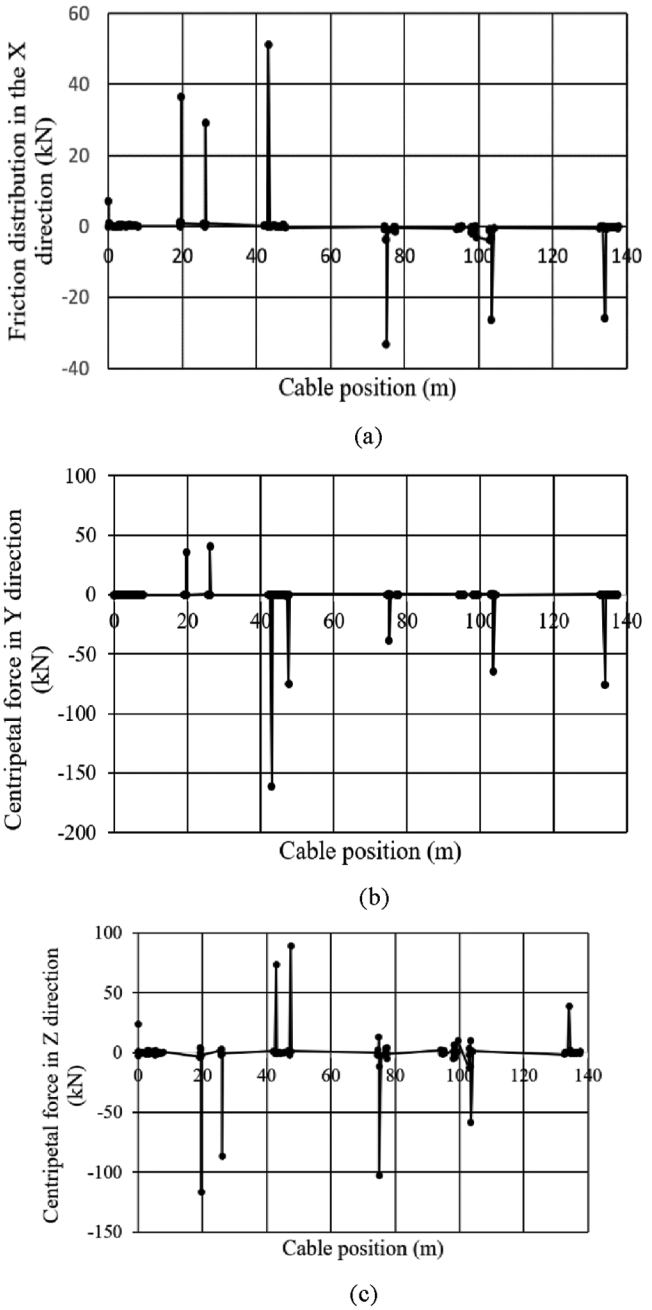

Fig. 8—(a) Friction distribution in x-direction; (b) centripetal force in y-direction; and (c) centripetal force in z-direction.

A sectional force comparison is shown in Table 4. The table shows the characteristics of the results, including that

Table 4—Comparison of cross-sectional forces calculated by conventional analysis and proposed method for prestressing of all external cables (sectional force)

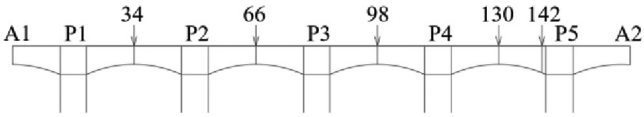

Section	Sectional force	Proposed method	Conventional method	Conventional/ Proposed	Section	Sectional force	Proposed method	Conventional method	Conventional/ Proposed
A1	Reaction force R_x, kN	0	—	—	130	Axial force N, kN	–35,458	–34,136	0.96
	Reaction force R_y, kN	0	—	—		Shear force (vertical) S2, kN	8	369	46.13
	Reaction force R_z, kN	–508	–577	1.14		Shear force (lateral) S3, kN	1770	—	—
	Moment M_x, kN·m	713	—	—		Torsional moment M1, kN·m	117	—	—
	Moment M_y, kN·m	–122	—	—		Bending moment M2, kN·m	–12,659	–14,270	1.13
	Moment M_z, kN·m	0	—	—		Bending moment M3, kN·m	–1604	—	—
34	Axial force N, kN	–35,245	–33,525	0.95	142	Axial force N, kN	–34,835	–34,194	0.98
	Shear force (vertical) S2, kN	–310	–320	1.03		Shear force (vertical) S2, kN	–1724	–719	0.42
	Shear force (lateral) S3, kN	–143	—	—		Shear force (lateral) S3, kN	–2773	—	—
	Torsional moment M1, kN·m	120	—	—		Torsional moment M1, kN·m	4121	—	—
	Bending moment M2, kN·m	–12,530	–13,932	1.11		Bending moment M2, kN·m	75,683	80,222	1.06
	Bending moment M3, kN·m	5320	—	—		Bending moment M3, kN·m	1301	—	—
66	Axial force N, kN	–28,231	–26,613	0.94	A1	Reaction force R_x, kN	0	—	—
	Shear force (vertical) S2, kN	–398	–113	0.28		Reaction force R_y, kN	0	—	—
	Shear force (lateral) S3, kN	–560	—	—		Reaction force R_z, kN	–96	–152	1.58
	Torsional moment M1, kN·m	–221	—	—		Moment M_x, kN·m	–48	—	—
	Bending moment M2, kN·m	10,886	12,459	1.14		Moment M_y, kN·m	0	—	—
	Bending moment M3, kN·m	–1610	—	—		Moment M_z, kN·m	0	—	—
98	Axial force N, kN	–28,223	–26,619	0.94					
	Shear force (vertical) S2, kN	–15	–90	6.00					
	Shear force (lateral) S3, kN	1021	—	—					
	Torsional moment M1, kN·m	130	—	—					
	Bending moment M2, kN·m	–10,099	–11,845	1.17					
	Bending moment M3, kN·m	100	—	—					

cross-sectional torsion is automatically generated in the analysis by the proposed method, in addition to the two components of cross-sectional bending moment around the y-axis and the z-axis. Furthermore, the shear force is calculated in two directions of the cross section in the proposed 3-D analysis, while the shear force is only in one direction and the bending moment is only around the y-axis in the conventional analysis. Therefore, the amount of information is completely different. It may be appropriate to add that the ground rigidity at the base of each pier is given with equivalent spring element rigidity with the values of ground spring rigidity given in the 2-D calculation. The use of spring elements is simply due to the code's functional limits.

Table 4 shows the values of the shear force and torsional moment at the girder cross sections numbered 34, 66, 98, 130, and 142 to emphasize the 3-D effect in the stress calculation, where the predominant sectional force causes bending. The difference in the resulting shear force between the proposed analysis and the conventional analysis in these cross sections is large, and the proposed analysis gives a larger shear force. However, the value itself is small and may not be the determining factor for sectional dimensions. The vertical shear force S2 in cross section number 142 obtained by the proposed method appears larger than that obtained by the conventional method. The authors cannot argue whether the proposed method is more or less secure than the conventional method based on this fact alone because the direction of the shear force due to prestress is opposite to that of the shear force due to the dead load and live load, and the overall load effect is not considered here. In contrast, this is considered to be an example suggesting that the proposed analysis method can improve the accuracy of PC structure designs in the future. From a design point of view, there are cases where a large amount of information is meaningless, but regardless, due consideration must be given to the axial force, two-directional shear forces, bending moment around two axes, and torsional moment acting on the cross section in the case of a curved bridge design. Moreover, it is suggested that these cross-sectional forces can be control index values in structural design.

Table 5—Comparison of displacements calculated by proposed method and conventional analysis for prestressing of all external cables (displacement in mm)

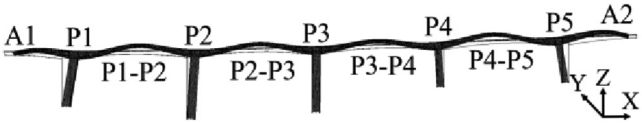

		Proposed analysis		Conventional analysis		Conventional/Proposed	
Direction	Axial	Vertical	Horizontal	Axial	Vertical	Axial	Vertical
A1	28.5	–0.4	3.4	22.0	0	0.77	0
P1	22.7	0	0.2	19.0	0	0.84	—
P1 to P2	18.0	19.6	0.7	13.5	20.8	0.75	1.06
P2	11.5	0	2.6	8.3	0	0.72	—
P2 to P3	7.0	17.2	4.1	3.9	18.9	0.56	1.10
P3	2.1	0	2.9	–0.5	0	–0.24	—
P3 to P4	–3.4	15.4	2.0	–4.9	18.4	1.44	1.19
P4	–6.9	0	0.3	–9.5	0	1.38	—
P4 to P5	–15.3	20.7	–0.6	–15.0	23.1	0.98	1.12
P5	–18.8	0	–1.1	–20.6	0	1.10	—
A2	–25.9	–0.7	–3.5	–24.0	0	0.93	0

In general, in any cross section, the axial force obtained using the conventional method is as small as approximately 90% of that using the proposed method, and the bending moment for the conventional analysis around the y-axis, M2, is always larger by approximately 10% than that for the proposed method. The reason for these tendencies may be the fact that the stiffness of the pier is smaller in the analysis by the proposed method due to the shear deformation effect, while the conventional method neglects this effect, resulting in stiffer pier deformational characteristics. This is observed in the displacement characteristics in the longitudinal direction. The displacement in the longitudinal direction is 30% larger at location A1 and 13% larger at location A2 in the proposed analysis; that is, the contraction of the upper box girder 462 m long is larger.

As for another trend of a larger bending moment, at almost all sections in Table 4 for the proposed method, with respect to the conventional calculation, the small deflection at every span center in the proposed calculation method may be related, as observed in Table 5. Further investigation of these phenomena is not discussed here and may be treated in future papers.

The one characteristic result to point out is that the bending moment around the z-axis, M3, exceeds the bending moment around the y-axis, M2, by 50% in section number 34, for which the conventional analysis gives no information, because M3 does not exist in the conventional calculation. The other characteristic point is that the torsional moment, M_x, is calculated in the proposed method, while in the conventional analysis, it is not. On this point, the Japan highway bridge design standard[3] specifies that it should be calculated in special cases by 3-D grid analysis using only the dead load of the bridge surface and live loads. However, the Japan bridge design standard[3] refers to this point as follows: "According to previous specifications, it is said that the effect of torsional moment due to live loads on straight single girders and T-girders is small, and it is not necessary to consider torsional moment. However, recent inspection results have confirmed cases of cracks occurring in bulkheads, etc., regardless of whether they are straight girders or curved girders, or regardless of cross-sectional dimensions, etc. and for which the influence of torsional moment cannot be denied. Therefore, the current design standard specifies that the torsional moment caused by live loads should be taken into consideration, as a principle of structural design."

Considering the previous results and requirements, the authors believe that the proposed method will be a more powerful tool for detailed structural analysis of prestressing large PC structures with a complex and arbitrary geometry.

OBSERVATION OF STRAIN DISTRIBUTION IN CABLES AND PULLED-OUT LENGTHS OF CABLES AT PRESTRESSING

Observation of strain distribution in cables between piers P2 and P4

As discussed earlier, the PC cable stress calculation is essentially the same in either calculation method because the following equation is used for cable stress calculation, and the same friction coefficients are used

$$\frac{\partial T}{\partial s} = \left(\mu \frac{\partial \theta}{\partial s} + \lambda\right) T \tag{19}$$

where T, s, and θ are the cable force, the length measured along the cable profile, and the directional angle change of the cable profile, respectively; and μ and λ are friction coefficients for the angle change and length change, respectively. However, the pulled-out cable length has scarcely been discussed in the past because it is affected by concrete contraction during prestressing. The initial stress method

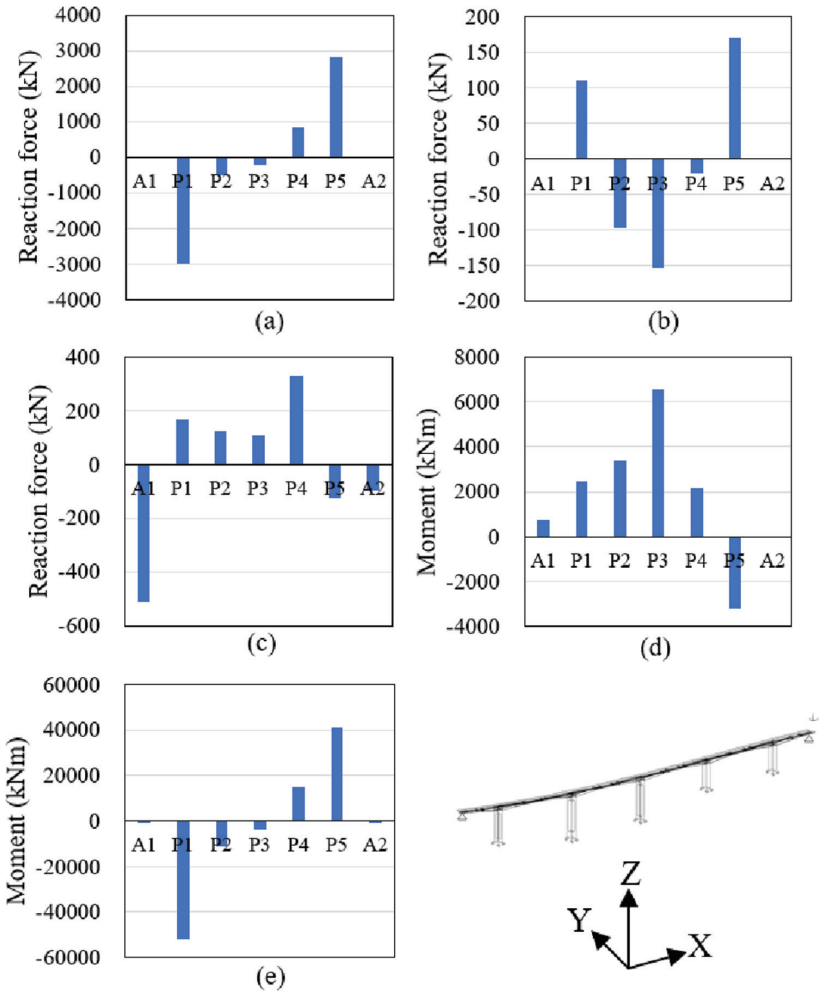

Fig. 9—(a) Axial ground reaction forces; (b) perpendicular ground reaction forces; (c) vertical ground reaction forces; (d) moment about bridge axis; and (e) moment perpendicular to bridge axis.

adopted in many types of software does not allow iteration of initial strain settings, even though the originally assumed initial strain cannot ensure a given pulled-out length after calculating the stress for related components. In contrast, the proposed method theoretically accounts for the seating loss mechanism and explains the measured strain distribution. Two cases of cable strain measurement for the bridge considered in the present study are discussed herein.

Strain measurement for cables was carried out for prestressing between piers P2 and P4. Similarly, the cable strain between P1 and P2 was measured with a similar embedded device. The difference between the two is that the cables between P2 and P4 are external cables and are surrounded by air for most of their length; therefore, the friction loss for the stress is mainly due to the angle change at the diaphragm wall in the span, while the cables between P1 and P2 are enclosed within the span, where friction loss occurs along their whole length. Figure 7 shows the cable profile between P2 and P4.

Table 6 shows the analysis conditions. Figures 10(a) and (b) show a comparison between the measured tension force in the prestressing cable and the analysis value. In Fig. 10, the cable where strain is measured is an external cable that is surrounded by air, except at the pier head and the diaphragm wall section. Despite the fact that the cable is surrounded by air, the measured strain varies in these exposed cable sections, which may not be reasonable. This seems to be due to a device error, and it limits the accuracy of the measurement. If these fluctuations are ignored, the calculation and measurement results are in good agreement when the friction coefficients are assumed to be $\mu = 0.3$ and $\lambda = 0.003$, and the pulled-out length in Table 7 is almost the same as the measured length. Seating analysis has rarely been discussed in the past. As shown in Fig. 10(a), the target bridge provides data for the strain distribution after seating, which indicates that the strain relief zone is extended over the whole span with a length of over 91 m, and this observation is quite contrary to the basic assumptions of the Japan highway standard[3] or DIANA manual, which assume a mirror inversion relief line of prestressing at a certain level that is determined so that the integrated strain value becomes a stipulated seating value. Note that at this stage, in prestressing design, it is necessary to identify critical sections where the stress becomes a maximum and a minimum along the span length of concern. The results show that these locations are completely different from those considered by the designer, which means that it is necessary to improve the seating analysis. For this purpose, a method must be used that can simulate the general seating stress distribution. Here, it is attempted to apply Eq. (19) with slight modification of the

Table 6—Analysis conditions (P2 to P4)

Item	Value	Remarks
Young's modulus	194,150 N/mm^2	From average of mill sheets
Prestressing force at end	3472.37 kN	From final tension of 40.7 MPa in prestressing management diagram, considering 1% of jack internal friction loss
Coefficient of friction	In air: λ = 0/m μ = 0/rad In concrete: λ = 0.003/m μ = 0.3/rad	From this study
Pulled-out length at anchorage	P2 side: 11.6 mm P4 side: 11.6 mm	From this study

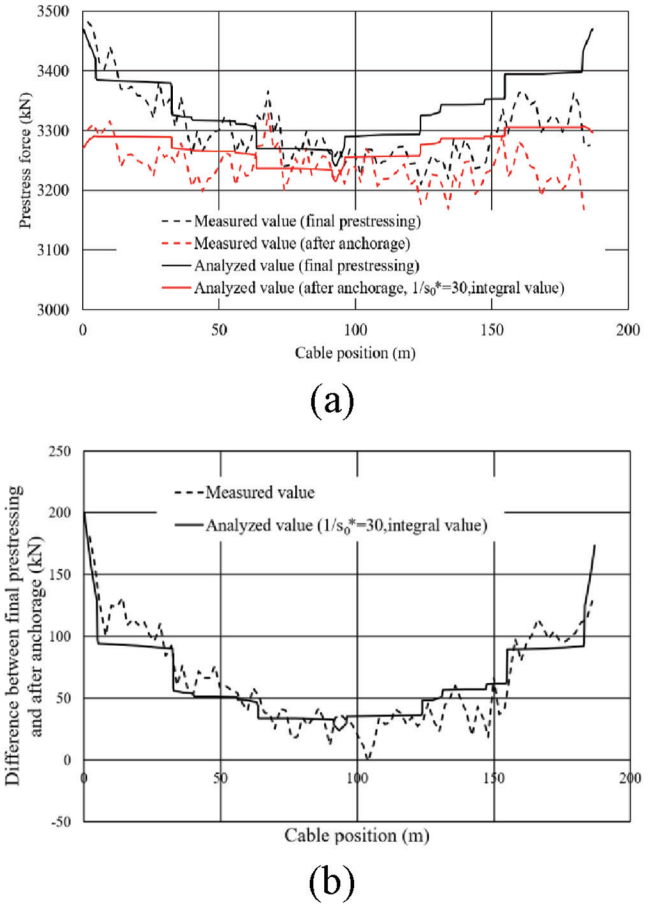

Fig. 10—(a) Comparison of measured and analysis values for prestressing force; and (b) comparison of measured and analysis values for difference between final prestressing and after anchorage (in cables between piers P2 and P4).

friction factors, assuming the superposition of much larger friction coefficients. The results are shown in Fig. 10(b). Note that the strain data represent the relieved portion of the total strain upon consideration that the observed total strain in the P2 to P4 side has some irregularity. The results show good agreement with the observed strain data, which suggests that stress relief for prestressing cables after seating may be possible with this analysis method.

Table 7—Comparison of PC cable pulled-out length (P2 to P4)

One side	Starting side	Measured value	613 mm
		Calculated value	604 mm
	Ending side	Measured value	610 mm
		Calculated value	619 mm
Both sides (total)		Measured value	1222 mm
		Calculated value	1223 mm

Herein, it may be necessary to elaborate on the assumption adopted in this seating analysis. The assumption is that the cable force is expressed at seating as follows

$$T = T_0 \cdot e^{-\mu\theta\left(\frac{s}{s_0^*}\right)-\lambda\left(\frac{s}{s_0^*}\right)} \quad (20)$$

where the original length s for the cables is normalized by s_0^* to express the contact point density, where s_0^* = 1 m in the original equation at prestressing and decreases at the seating stage according to the increase in its density. For the seating analysis of the P2 to P4 cables, s_0^* = 1/30 m was adopted. In other words, the contact length index s_0^* was taken as 3.33 cm.

Observation of strain distribution in cables between P1 and P2

For the strain measurement between P1 and P2, shown in Fig. 11, prestressing of this internal cable involved connecting the cantilever tip. This span connection is the last step in the closure of all spans, and the pulled-out length for the prestressing cables is affected by the structural rigidity of the entire bridge. The measured prestressing force for the PC cable during prestressing and after seating is shown in Fig. 12. The prestressing force on the P2 side appears to be larger than that on the P1 side. However, according to the prestressing management chart used during construction, the same prestressing force was introduced on both the left and right sides, and the difference between the measured values and the actual values is most likely due to the fact that the part of the PC cable arrangement that causes angle changes on the P1 side is not identical to that on the P2 side, or it is due to measurement error. It should also be noted that prestressing relief at seating occurred over the entire length of the PC cable, which is 36.08 m long, and the prestressing loss in the center of the PC cable was almost equal to that at the anchorage end.

The PC steel specifications used in the analysis are shown in Table 8. Young's modulus values were taken from the mill certificate issued by the material manufacturer to be aligned with on-site prestressing management records.

The measured values of the pulled-out length of the cable and the results calculated by the proposed method are shown in Table 9. The total calculated pulled-out length for the PC steel agrees well with the measured value.

A comparison of the PC cable force at prestressing and after seating between the observed values and the calculated values assuming friction coefficients of μ = 0.055 and λ = 0.0005 and the same contact length index s_0^* of 3.33 cm is

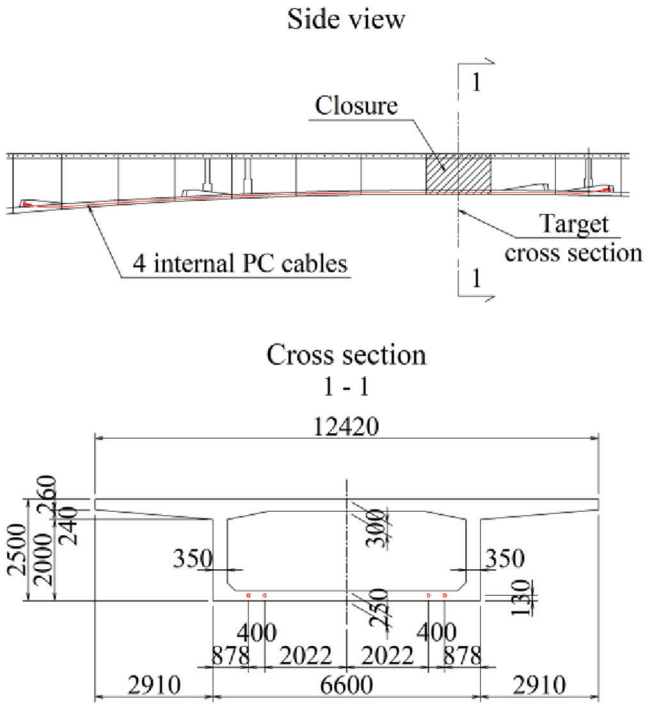

Fig. 11—Internal PC cables layout of P1 to P2 span for closure. (Note: Units are in mm.)

shown in Fig. 12. These results show almost perfect agreement between the observed and calculated strain values.

The original friction coefficients that should be adopted at prestressing need to be discussed in more detail. However, this remains a topic for future work.

IMPROVEMENT OF PRESTRESSING MANAGEMENT

Prestressing management in force-diverting systems

The induced prestress in large-scale structures is, in most cases, dependent on its indeterminate order because the jack prestressing force is distributed to related structural components to which the jack stressing component is connected.

Current management of prestressing in Japan adopts the jack pressure and pulled-out length for a cable from an anchor plate as the control indexes for prestressing, though practices outside Japan seem to adopt jack pressure alone.

The pulled-out length criterion, $\Delta_s + \Delta_c$, is the sum of the cable elongation and concrete contraction. However, concrete contraction Δ_c cannot be calculated yet using the tools presently available. Therefore, a certain amount of error always exists in the current calculations because the current management method neglects this factor, and the rigidity of cables less than the actual values is specified in a rather obscure form in the Japan Road Association standard.[3]

The concrete deformation due to prestressing, Δ_c is expressed as

$$\Delta_c = \int_{s_0}^{s} \varepsilon_c \, ds \tag{21}$$

where integration is carried out along the cable profile to the end point, starting from the unique unmovable point where the concrete and cable have no relative slip. The method

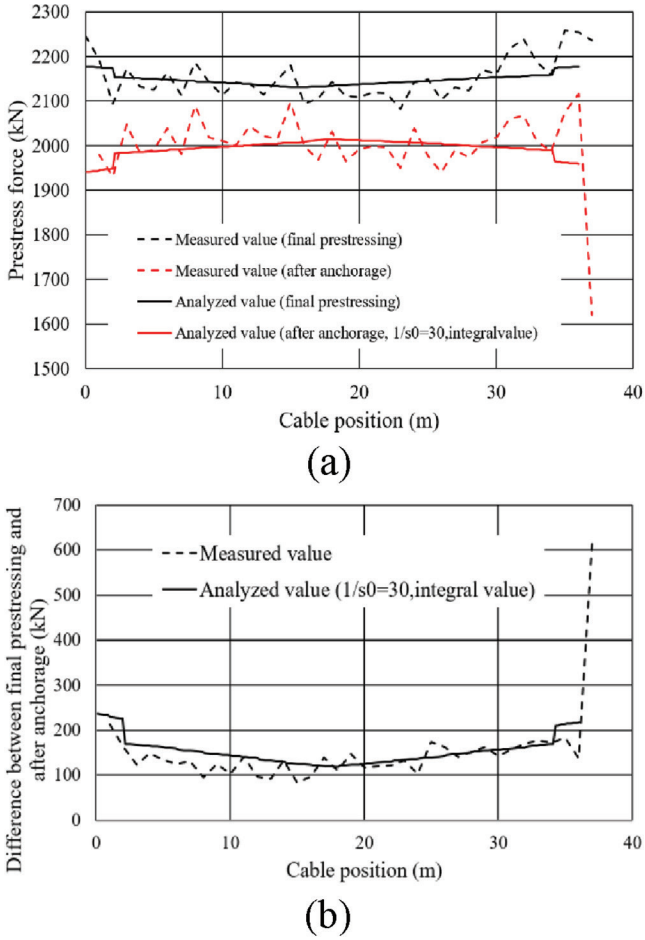

Fig. 12—(a) Comparison of measured and analysis values for prestressing force; and (b) comparison of measured and analysis values for difference between final prestressing and after anchorage (in cables between piers P1 and P2).

Table 8—Analysis conditions (P1 to P2)

Item	Value	Remarks
Young's modulus	191,900 N/mm^2	From average of mill sheets
Prestressing force at end	2177.13 kN	From final tension of 40.0 MPa in prestressing management diagram, considering 1% of jack internal friction loss
Coefficient of friction	In concrete: λ = 0.0005 1/m μ = 0.055 1/rad	From this study
Pulled-out length at anchorage	P2 side: 8.6 mm P4 side: 8.6 mm	From this study

Table 9—Comparison of PC cable pulled-out length (P1 to P2)

One side	Starting side	Measured value	120 mm
		Calculated value	107 mm
	Ending side	Measured value	122 mm
		Calculated value	138 mm
Both sides (total)		Measured value	242 mm
		Calculated value	245 mm

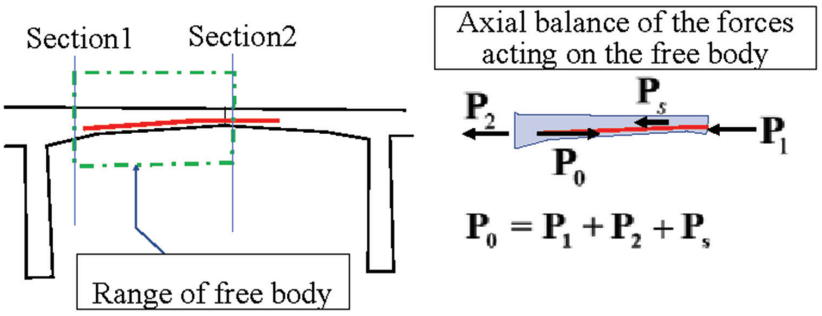

Fig. 13—Conceptual diagram of P1 to P2 prestressing force.

proposed in a previous paper[1] enabled the calculation of this contraction, and the pulled-out length can be correctly calculated and used for prestressing management.

Diverting prestressing force in actual six-span elevated bridge

As already discussed, the prestressing force branches off toward several components in indeterminate structures, as is shown for the target bridge, and the design jack prestressing force is not concentrated entirely in a design section. This situation is examined for an actual six-span bridge.

The prestressing force to close the span between piers P1 and P2 was examined by determining how much of the jack prestressing force is actually transferred to the closing section with respect to the design closing force. As shown in Fig. 13, the jack prestressing force P_0 is expressed as

$$P_0 = P_1 + P_2 + P_s = P_1 + \beta P_0 + (1 - e^{-\mu\theta-\lambda s})P_0 \quad (22)$$

where P_1, P_2, and P_s are the closing force at the closing section, the diverting force that acts on neighboring components, and the frictional force consumed between the jack point and the closing section, respectively; and the value β is a sensitivity factor, which is the ratio of the diverting force P_2 that acts on neighboring components having a jack prestressing force P_0. For this bridge, the closing cables for the span between P1 and P2 are set in two sections, with four cables per section. The total force for four cables is

$$P_0 = 8708.4 \text{ kN}$$

and the calculated values are

$$P_1 = 7853.7 \text{ kN}, P_2 = 380.2 \text{ kN}, P_s = 474.5 \text{ kN}$$

using the respective friction coefficients

$$\lambda/\mu = 0.0636, \mu = 0.055, \lambda = 0.0035$$

P_2 is the portion of the jack force transferred to neighboring components, which are subjected to 4.4% of the jack prestressing force. Adding up the frictional loss from P_2 and P_s shows that almost 10% of the jack prestressing force is not used for the closing span, and approximately 90% of the jack prestressing force acts as the closing force. This is an assumed force distribution, which depends on the assumed rigidity of the base ground and pier and the friction coefficients, and there is no assurance that all the parameters in the calculation are correct. Among these parameters, the one most likely to vary is the ground rigidity, which changes to half or twice the assumed value rather easily. Therefore, it is proposed that the effect should be closely examined for proper prestressing management. There are at least three major parameters—β, μ, and λ—that affect the accuracy of the working force at a design section, and determining the sensitivity of the parameter β to the ground rigidity may be most important and has been performed for the target bridge.

The sensitivity to β is defined in this study such that the β value varies when the ground rigidity changes within the range of +50% to –50% of the design value. Therefore, numerical prestressing experiments were performed while multiplying the design value of the ground rigidity twice by a factor of 1/1000. The results are shown in Fig. 14 and 15.

In Fig. 14, the horizontal axis is the number of multipliers for the assumed ground rigidity, and the vertical axis is the concrete contraction at the jack point. In Fig. 15, the horizontal axis is the number of multipliers for the assumed ground rigidity, and the vertical axis is the β value.

The β value with the assumed ground rigidity is given by

$$\beta = 380.2 \text{ kN}/8708.4 \text{ kN} = 0.044 = 4.4\%$$

Figure 15 shows that when the ground rigidity changes from approximately 1.5 times to 0.5 times, the β values only exhibit a small variation of 0.042%. Thus, the sensitivity to ground rigidity variation in this case is only 4.2%, which indicates that it does not much affect prestressing force transfer to the design section in this case. This is an indication that the ground is hard enough, and changing the rigidity to half of the initial value will affect the prestressing force at the section by only 4.2%. The ground on which the bridge was constructed seems to have rather high soil rigidity, and it can be safely assumed that a variation in the assumed ground rigidity by approximately 1.5 or 0.5 times the initial value does not affect the prestressing force applied to the closing section.

Proposed prestressing management

Prestressing management is a kind of remote management for introducing force to a cross section several tens of meters away from a jack point, during which the frictional jack force is reduced. Moreover, for structures with a large number of indeterminate orders, the jack prestressing force is diverted to many structural components, and identification of the force transferred to the design cross section depends

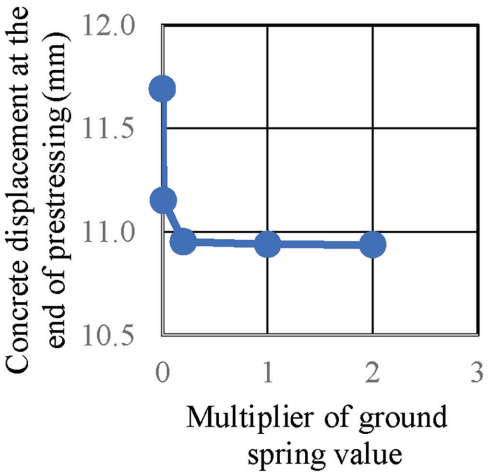

Fig. 14—Sensitivity of concrete displacement to ground rigidity.

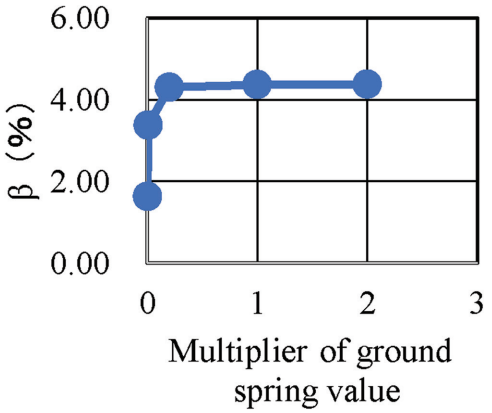

Fig. 15—Sensitivity of ground spring value β to ground rigidity multiplier.

on the accuracy of the analytical calculation. Based on these considerations, the proposals for improving the management of prestressing are as follows:

1. The sensitivity of the β value to ground rigidity is first examined. However, if other factors influence the ground rigidity, then a sensitivity study must be carried out for these factors as well.

2. A prestressing management chart is drawn with a horizontal axis that is the pulled-out length for the cable from the anchor plate, $\Delta_s + \Delta_c$, while the vertical axis is the jack pressure—that is, the prestressing force. In the chart, a stop line for prestressing is drawn. This line is directly affected by the β value, because the prestressing force acting at the target section P_1 is

$$P_1 = \xi P_0$$
$$\xi = e^{-\mu\theta-\lambda s} - \beta \quad (23)$$

as shown conceptually in Fig. 16.

3. The measured slope of the pulled-out length for the cable is matched with the chart slope to determine the specific μ and λ values.

4. The value of ξ may be estimated by an appropriate strain measurement device in the upper and lower box slabs.

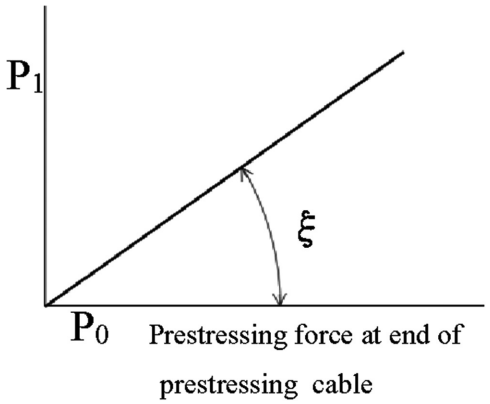

Fig. 16—Conceptual diagram of influence factor.

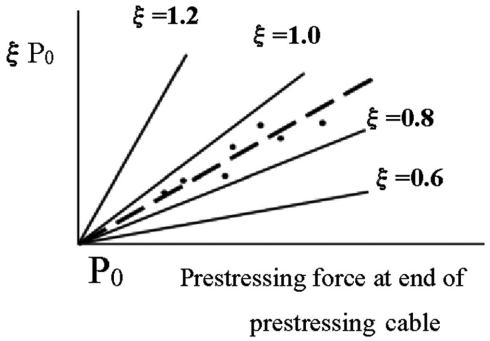

Fig. 17—Conceptual diagram of β identification.

5. If the estimated ξ is outside the limit range, then β should be reestimated from Fig. 17.

Therefore, the prestressing management chart is almost similar to the current chart commonly used.[8] However, the value of β should be written in the chart with μ and λ.

For variations in the β value outside the limit range, the standard should specify how to cope with this situation.

CONCLUSIONS

To extend a study reported in a previous paper,[1] the developed three-dimensional (3-D) finite element method (FEM) was enhanced to compare its theoretical basis with that for the initial strain method. The resulting FEM was applied to a prestressing calculation for an existing six-span, 462 m long bridge, and the observed strain distribution in the cables was compared with the calculated values even after the seating stage, which showed that the current seating loss analysis needs major revision. Based on the results obtained, a new prestressing management method was proposed to ensure the reliability of constructed prestressed concrete (PC) structures.

AUTHOR BIOS

Hiroshi Nishio *is the former Representative Director and Executive Vice President of ABE NIKKO KOGYO CO., LTD. He received his master's degree in engineering from Tohoku University, Sendai, Japan.*

Yosuke Yagi *is an Executive Officer at Fuji P.S Corporation. He received his BS from Meijo University, Nagoya, Japan.*

Yasuaki Ishikawa *is a Professor at Meijo University. He received his DrEng from Nagoya University, Nagoya, Japan. His research interests include the mechanical behavior of prestressed concrete structures and its numerical simulation.*

ACKNOWLEDGMENTS

This study was conducted as part of the research activities of the LECOM Study Group. Thanks are due to T. Tanabe, Professor Emeritus of Nagoya University, and the study group members T. Endo, Professor Emeritus of Tohoku Gakuin University, and Y. Sasaki of the Japan Ministry of Land, Infrastructure, Transport and Tourism. Thanks are also due to H. Osawa, K. Temamoto, and N. Sogabe, Kajima Corporation, for providing valuable data, including optical fiber measurement data. Finally, thanks go to Y. Imai of Fuji Consultants for providing information on overseas prestressing management.

NOTATION

$\boldsymbol{F}_i$	=	jack, frictional, and other forces
$N_{rm}N_x$, $N_{rm}N_y$, $N_{rm}N_z$, $N_{rm}M_x$, $N_{rm}M_y$, $N_{rm}M_z$	=	error norm
N_x, N_y, N_z	=	nodal forces of elements
P_s	=	frictional force consumed between jack point and closing section
P_0	=	jack prestressing force
P_1	=	closing force at closing section
P_2	=	diverting force that acts on neighboring components
s	=	length measured along cable profile
T	=	cable force and directional angle change for cable profile
$\boldsymbol{u}_i$	=	measured from any point in space
β	=	sensitivity factor for diverting force P_2 acting on components' neighboring jack with prestressing force P_0
Δ_c	=	sum of all concrete contraction
Δ_s	=	sum of all cable elongation
γ	=	shear strain of section
λ	=	frictional coefficient for length change
μ	=	frictional coefficient for angle change
θ	=	directional angle change for cable profile
ξ	=	sensitivity factor for closing force at closing section P_1 acting on components' neighboring jack with prestressing force P_0

REFERENCES

1. Ishikawa, Y., and Watanabe, K., "A Numerical Study on the Accuracy of Prestressing Analysis with Initial Strain Method," The 79th JSCE Annual Meeting Proceedings, Japan Society of Civil Engineers, Tokyo, Japan, 2024.

2. Ishikawa, Y.; Nishio, H.; and Yagi, Y., "Development on New 3DFEM Analytical Method and Management in Prestressing Process for PC Structures," *Journal of Japan Society of Civil Engineers*, V. 79, No. 10, 2023, Article No. 23-00003. doi: 10.2208/jscejj.23-00003

3. Japan Road Association, "Specification for Highway Bridges Part III Concrete Bridges," Tokyo, Japan, 2017.

4. Okubo, K.; Imai, M.; Sogabe, N.; Nakaue, S.; Chikiri, K.; and Niwa, J., "Development of the Measuring Method for PC-Tensile Force Distribution by Optical Fiber Applicable to Control of Prestressing and Maintenance of PC Structures," *Journal of Japan Society of Civil Engineers Ser. E2 (Materials and Concrete Structures)*, V. 76, No. 1, 2020, pp. 41-54. doi: 10.2208/jscejmcs.76.1_41

5. Nagumo, H.; Mouri, K.; Morita, Y.; Sogabe, N.; Imai, M.; and Sato, T., "Construction of Tsukidate Viaduct Superstructure as Part of Reconstruction Assistance Road," *Bridge and Foundation Engineering*, V. 50, No. 12, 2016, pp. 5-10.

6. FORUM8, "UC-BRIDGE," Version 10, FORUM8 Co., Ltd., Tokyo, Japan, 2023.

7. JIP Techno Science Corporation, "PCBOX-II," Version 2018.5.8, Tokyo, Japan, 2018.

8. Ishii, T.; Kikuchi, A.; and Itaya, H., "Consideration on Effectiveness of Elongation Measurement System for Prestressing Using Image Processing Technology," *Proceedings of the 29th Symposium on Developments in Prestressed Concrete of Japan Prestressed Concrete Institute*, 2020, pp. 453-456.